Geometric Positioning Error Mitigation of SAR Image in Ocean Utilizing AIS Information

Juyoung Song, *Student Member, IEEE*, Duk-jin Kim, *Senior Member, IEEE*, Seungwoo Lee, Sangho An, Ji-Hwan Hwang, and Junwoo Kim

***Abstract*— Mitigation of geometric calibration offset in ocean without utilizing ground control points (GCPs) was investigated in this study. Real-time automatic identification system (AIS) information on vessels was exploited after preprocessing and accordingly tested against the detected vessels in the synthetic aperture radar (SAR) image. A repetitive procedure of measuring the offset between the AIS sensor and the vessel detection was conducted and derived the SAR image of which the positioning offset was ameliorated. The proposed geo-location enhancement algorithm demonstrated the possibility of application in real-time vessel monitoring from remote sensing.**

***Index Terms*— Automatic identification system (AIS), ellipsoid correction, geometric calibration, synthetic aperture radar (SAR), vessel detection.**

I. Introduction

GEOMETRIC positioning accuracy is crucially influenced by the acquisition geometry of remote sensing apparatus; the discrete location, velocity, and motion of the sensor are required to be measured precisely [1]. Due to the demand for enhancing positioning accuracy, advanced geo-location sensors such as global navigation satellite system (GNSS) and inertial measurement unit (IMU), respectively, estimating the location with velocity and geometric motion, were introduced and implemented to the sensor [2]. In order to enhance the acquisition of location, velocity, and motion, suppression of intrinsic measurement error terms was generally applied through the Kalman Filter, utilizing the covariance matrix of the maneuvering target sensor [3]. The procedure of allocating an exact coordinate location, notably longitude and latitude, is acknowledged as geometric calibration; either the surface elevation in the form of a digital elevation model (DEM) can be implemented, or simply utilizing the Earth ellipsoid [4]. The geometric calibration with and without surface height information is respectively entitled terrain correction and ellipsoid correction.

Manuscript received 28 November 2022; revised 14 February 2023; accepted 24 February 2023. Date of publication 7 March 2023; date of current version 16 March 2023. This work was supported in part by the National Research Foundation of Korea (NRF) through the Ministry of Science and ICT under Grant 2021R1A2C2006025; and in part by the Unmanned Aerial Vehicle (UAV)-Based Marine Safety, Illegal Fishing and Marine Ecosystem Management Technology Development through the Ministry of Ocean and Fisheries (MOF), South Korea, under Grant 20190497. *(Corresponding author: Duk-jin Kim.)*

The authors are with the School of Earth and Environmental Sciences, Seoul National University, Seoul 08826, South Korea (e-mail: 96daniel@snu.ac.kr; djkim@snu.ac.kr; ert0706@snu.ac.kr; hoo89336@snu.ac.kr; hwang1651@snu.ac.kr; darkcroa@snu.ac.kr).

Digital Object Identifier 10.1109/LGRS.2023.3253775

Residual geo-location error was generally suppressed using ground control points (GCPs), conspicuous ground targets whose location was measured by rigorous land surveying [5]. For ocean remote sensing, however, accurate geometric calibration and its amelioration from DEM and GCP were limited [6]. It impeded the robust application of using remotely sensed data in which the precise estimation and indication of marine target location were necessary, including vessels and man-made stationary structures [7]. For monitoring vessels in ocean, identifying the accurate position is highly demanded in reaction against illegitimate fishing activities [8]. Monitoring vessels for marine security from remotely sensed image was conducted by means of detection, which was conventionally conducted from convolutional neural network (CNN) based object detector, as an optimized image analyzer for image pattern recognition [9], [10].

Among remote sensing apparatus, synthetic aperture radar (SAR) is appreciated for its stability of acquisition which facilitates periodic monitoring of identical region of interest and weather independency [5]. High expectation of data procurement in a regular manner enabled SAR remote sensing to be utilized in vessel surveillance in a specific region of ocean, particularly when a time-series analysis of vessel position was necessary [8]. Detected vessels in SAR image were often incorporated with automatic identification system (AIS) data: real-time monitoring information of vessel which discretely contains its position and velocity [11]. Nevertheless, due to the mismatch between the acquisition time of SAR and AIS, AIS information ought to be preprocessed with respect to SAR data before use. AIS information demonstrated its precision of approximately 3 m even when the vessel was moving, when tested against real-time kinematic (RTK) sensor [12].

Implementing geometric calibration of remotely sensed image without using terrain information not only causes considerable positioning offset but also impedes the accurate recognition of ocean man-made targets. In order to enhance the geometric calibration of SAR image in which GCP analyses were limited and to enable the precise indication of vessel position in ocean for its practical and robust surveillance from remotely sensed data, an algorithm which mitigates the position deviation of SAR image after geometric calibration utilizing AIS information was proposed. Ascertainment of the algorithm's robustness was attested using two different types of conventional satellite SAR data along with that of small SAR satellite operating with constellation.

II. Data Acquisition and Preprocessing

A. Ellipsoid Correction of SAR Image

Ellipsoid correction rendered a projection of SAR single look complex (SLC) image on the Earth ellipsoid regardless of its acquisition from satellite or aircraft [4]. Range-Doppler model was widely used in matching the position of each target pixel (T_x, T_y, T_z) from three different equations: Doppler equation, Range equation, and Ellipsoid equation.

Doppler equation defines the azimuth plane from Doppler centroid. From the derivative of SLC phase, Doppler centroid f_{DC}, intercept of linear Doppler history is denoted as follows, using relative range vector $\boldsymbol{R_r}$ from sensor to target, velocity vector $\boldsymbol{v_r}$, and radar wavelength λ_0:

$$f_{\mathrm{DC}} = \frac{2\boldsymbol{R_r} \cdot \boldsymbol{v_r}}{\lambda_0 |\boldsymbol{R_r}|}. \tag{1}$$

Doppler centroid is often predicted with respect to the Earth rotation and sensor movement [13]; as each range pixel i_τ and azimuth pixel i_η in radar coordinate demonstrate different Doppler centroid, a lookup table was generated with respect to range and azimuth bin. From (1), Doppler equation is derived as follows, finding the point of (T_x, T_y, T_z) which determines $\boldsymbol{R_r}$:

$$A_1(i_\tau, i_\eta) = f_{\mathrm{DC}} - \frac{2}{\lambda_0 |\boldsymbol{R_r}|}(\boldsymbol{R_r} \cdot \boldsymbol{v_r}) = 0. \tag{2}$$

Given that SAR system exploits the time delay in measuring the distance, Range equation in (3) denoted the range bin position from range time response with respect to each azimuth time bin. The notations δ_r and Δ_r respectively express range offset and slant range spacing

$$A_2(i_\tau, i_\eta) = \delta_r - \Delta_r i_\eta - |\boldsymbol{R_r}| = 0. \tag{3}$$

As the Earth was able to be simplified as an ellipsoid with semi-major axis r_a and semi-minor axis r_b, desired point (T_x, T_y, T_z) is placed on the ellipsoid as follows:

$$\frac{T_x^2 + T_y^2}{r_a^2} + \frac{T_z^2}{r_b^2} = 1. \tag{4}$$

Searching the geo-location for each point which satisfies (2)–(4) leads to a projection of radar coordinate to geographic coordinate. As residual error terms were generated from instantaneous squint angle and relative motion between the Earth rotation and the antenna [13], sensor measurement precision is significant in ellipsoid correction accuracy. This study, therefore, utilized three different SAR satellite sensors: 1) two different conventional satellite SAR sensors, COSMO-SkyMed Himage mode with 3 m resolution and Sentinel-1 interferometric wide (IW) mode with 20 m resolution and 2) a small SAR satellite with mass constellation, HiSEA-1 with 1 m resolution [14], [15]. Given that small SAR systems use compact measurement sensors, it is expected that the accuracy of ellipsoid correction accuracy is lower than that of conventional satellite SAR systems. The coverage of SAR image data for assessing geo-location amelioration and the posts of land surveying are described in Fig. 1.

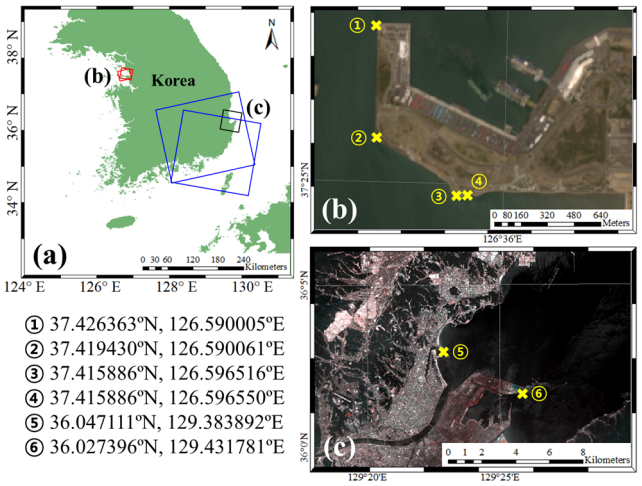

Fig. 1. (a) Study area of satellite SAR data. Red, black, and blue rectangles denote the spatial coverage of HiSEA-1, COSMO-SkyMed, and Sentinel-1, respectively. The reference control points in yellow index were selected in vicinity of the pier of (b) Incheon and (c) Pohang to assess the geometric calibration offset mitigation algorithm. The satellite images in (b) and (c) were acquired from Sentinel-2.

B. Vessel Detection and AIS Preprocessing

Before comparing real-time AIS information and geo-located SAR images, AIS information acquired in vicinity of region of interest and SAR acquisition time was preprocessed with respect to SAR acquisition time. Comprised of location, velocity, and vessel specification with AIS sensor spatial allocation, each piece of AIS information was acquired discretely. As proposed by Song et al. [8], matching the AIS information to remotely sensed image acquired for a continuous time was identically implemented, in order to identify the precise location of AIS sensor in image coordinate.

After ellipsoid correction, acquisition time array was generated for respective SAR image. First, a uniform interpolation was implemented to all vessels in image scene with respect to mean SAR imaging time. For each vessel, point in image coordinate after interpolation was defined and corresponding SAR acquisition time was then configured. Interpolation was performed accordingly using the renovated target interpolation time for each vessels. It was repeatedly performed until the interpolation took place within the platform spatial resolution.

In addition, azimuth focusing displacement due to the target velocity was additionally corrected. With target range velocity v_y and radar platform velocity v_a, azimuth focusing displacement δ_x is elaborated as follows [8]:

$$\delta_x = \frac{v_y}{v_a} |\boldsymbol{R_r}|. \tag{5}$$

Range velocity of each target vessel was derived from interpolation of AIS velocity, while slant range $|\boldsymbol{R_r}|$ was estimated from the restoration of SAR platform path using state vector and their respective orbital elements [8].

Detection of vessels in ellipsoid corrected SAR image was conducted by means of CNN-based object detector, you only look once version 4 (YOLOv4) for accuracy and processing time [16]. Training of the vessel detector was conducted using 33 HiSEA-1 spotlight COSMO-SkyMed Himage mode

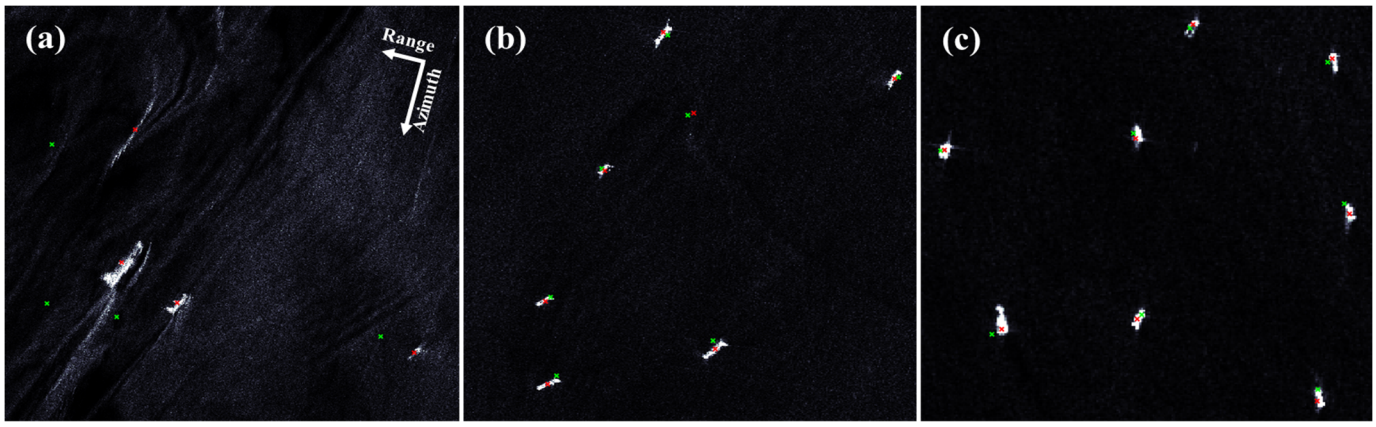

Fig. 2. Typical example of the geometric positioning offset in different SAR images acquired from descending orbit, where red and green indexes respectively indicate the detected vessel center and preprocessed AIS information. (a) HiSEA-1 acquired on April 12, 2022. (b) COSMO-SkyMed acquired on July 22, 2018. (c) Sentinel-1 acquired on December 6, 2018.

TABLE I
VESSEL DETECTION PERFORMANCE ON DIFFERENT SAR IMAGES UTILIZING THE CNN-BASED VESSEL DETECTOR

SAR Satellite	Precision	Recall	F1
HiSEA-1	76.92%	73.17%	75.00%
Cosmo-SkyMed	75.58%	67.12%	71.10%
Sentinel-1	82.98%	83.28%	83.13%

images and 31 Sentinel-1 IW mode images; validation was performed from four HiSEA-1 images, three COSMO-SkyMed images, and five Sentinel-1 images. SAR images for training and validation were separately used from those for verifying the effectiveness of geo-location enhancement. Assessment parameters of precision, recall, and their harmonic mean $F1$ score were utilized in order to evaluate the detection performance. Precision and recall were calculated from (6) and (7), by averaging the performances of SAR satellite images for validation. The notations n_a, n_d, and n_t indicate the number of accurately detected targets, total detected targets, and actual targets in the scene

$$\text{Precision} = \frac{n_a}{n_d} \tag{6}$$

$$\text{Recall} = \frac{n_a}{n_t}. \tag{7}$$

Table I describes the detection results on three different types of SAR satellite, Sentinel-1, COSMO-SkyMed, and HiSEA-1. Utilizing them, vessels were equally detected on four Sentinel-1 IW mode images, five COSMO-SkyMed Himage mode images, and 23 HiSEA-1 spotlight mode images for operation of geo-location enhancement. Fig. 2 demonstrates the examples of geometric positioning offset in SAR images, and the difference between the detected vessel center and preprocessed AIS sensor location.

III. METHODOLOGY

A. Repetitive Geometric Positioning Offset Calibration

This study presented a mitigation of geometric calibration utilizing the location of detected vessels in image coordinate and preprocessed AIS information. The presented algorithm exploits the character of AIS positioning sensor whose positioning offset was less than 3 m even when the vessel was moving [12]. Such accuracy signified that precisely preprocessed AIS information well represents the authentic location, than that of SAR image.

Unlike AIS information, the reference of SAR image was susceptible to geo-location error, caused by measurement error of sensor platform [13]. As the vessel detection was conducted on SAR images after ellipsoid correction, the detected vessels were equally influenced by geometric calibration error; AIS information projected to the image coordinate did not accurately represent the corresponding vessel signal. Hence, offset between the detected vessels and projected AIS information on image signified the quantity of offset from ellipsoid correction.

The detected vessel position indicated as a bounding box was reduced to its center, which demonstrated the vessel point location in SAR image coordinate. The distance range to compare the distance between AIS position and that of detected vessel, search radius, was defined; AIS response without vessel detection or detected vessel not identified by AIS information had a risk of causing estimation error while implementing geo-location error mitigation. Search radius was determined utilizing the distribution of AIS-monitored vessels in the SAR image. From all possible distances between the preprocessed AIS points, third quartile was selected as a search radius rather than the largest distance in order to keep the isolated AIS signal from degrading the offset estimation. With respect to preprocessed AIS information, the gap toward that of detected vessels inside a search radius was measured; the smallest length of separation was selected among them.

After estimating the distance to the nearest detected vessel, the latitude and longitude components of every offset were respectively averaged. The SAR image geographic coordinate was then modified such that the mean disparity in latitude and longitude was calibrated. Using the renovated SAR image coordinate, AIS information was converted to image coordinate and accordingly tested against the detected vessels. It was

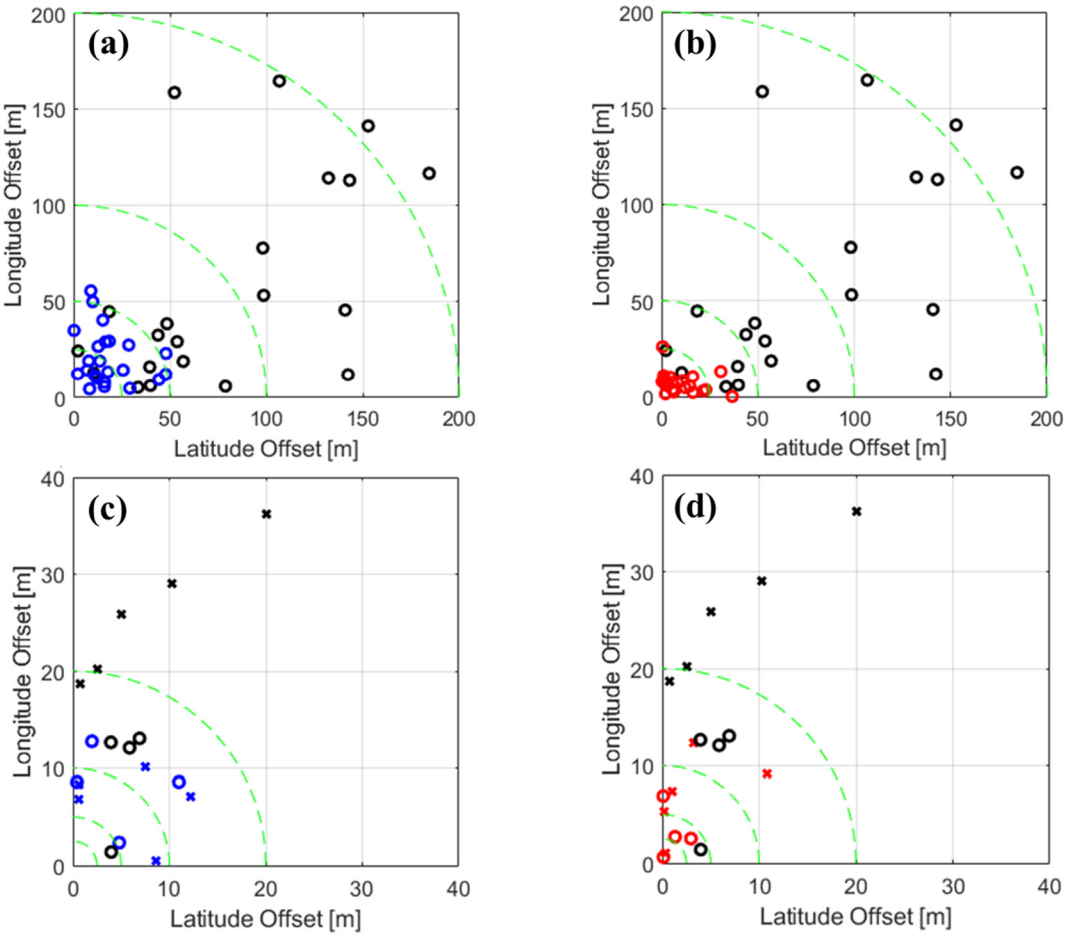

Fig. 3. Measurement on geo-location offset using (a) and (b) 23 HiSEA-1 images and (c) and (d) four Sentinel-1 and five COSMO-SkyMed images. Black, blue, and red colors respectively signify the ellipsoid correction, enhancement without and with static AIS information. Notations in circle and cross each denote Sentinel-1 and COSMO-SkyMed images in (c) and (d). Green dashed lines denote 200, 100, 50, and 25 m of offset for (a) and (b) and 20, 10, 5, and 2.5 m for (c) and (d).

repeatedly performed until the average offset of a certain iteration was not shifted more than a spatial resolution. The image after this procedure signified the offset calibrated SAR data with respect to AIS positioning sensor.

B. Correction of AIS Sensor Arrangement

Static AIS information of each vessel included dimension, the distance from the AIS positioning sensor to stem, bow, port, and starboard, which indicates the immutable character of each vessel [11]. Aside from the detected vessel in image coordinate whose position was arranged in the middle, AIS sensors were not always centered inside the vessel. Utilization of the dimension, representing the arrangement of AIS positioning sensor in the vessel, was proposed to resolve this issue; estimation of the vessel center was performed from its length and width.

The relation between AIS sensor position in vessel and its center was driven as (8) and (9), where (x_b, y_b) and (x_c, y_c) respectively signify the AIS sensor location and the vessel center in image coordinate, DimA − D denotes length from the AIS sensor to bow, stem, port, and starboard and θ indicates the modulus of COG bounded from 0 to $\pi/2$

$$x_c = x_b + \frac{\text{DimA} - \text{DimB}}{2}\sin\theta - \frac{\text{DimC} - \text{DimD}}{2}\cos\theta \quad (8)$$

$$y_c = y_b - \frac{\text{DimA} - \text{DimB}}{2}\cos\theta - \frac{\text{DimC} - \text{DimD}}{2}\sin\theta. \quad (9)$$

Two different cases with and without using static AIS information from (8) and (9) were equally ascertained for three different types of satellite SAR data. A comparison with the land surveyed control points was then performed.

IV. Results and Discussion

Iterative operation of geo-location offset estimation and its calibration on SAR images were performed on SAR images acquired from HiSEA-1, COSMO-SkyMed, and Sentinel-1. Two different enhancements of restraining the offset caused by the arrangement of the AIS positioning sensor in the vessel were equally implemented. The enhancement of SAR image geo-location for three different types of satellite SAR sensors is presented in Fig. 3. For small SAR satellite HiSEA-1, average geo-location error 109.10 m after ellipsoid correction was reduced to 27.41 m without using vessel dimension and 12.26 m with static AIS information. When assisted by

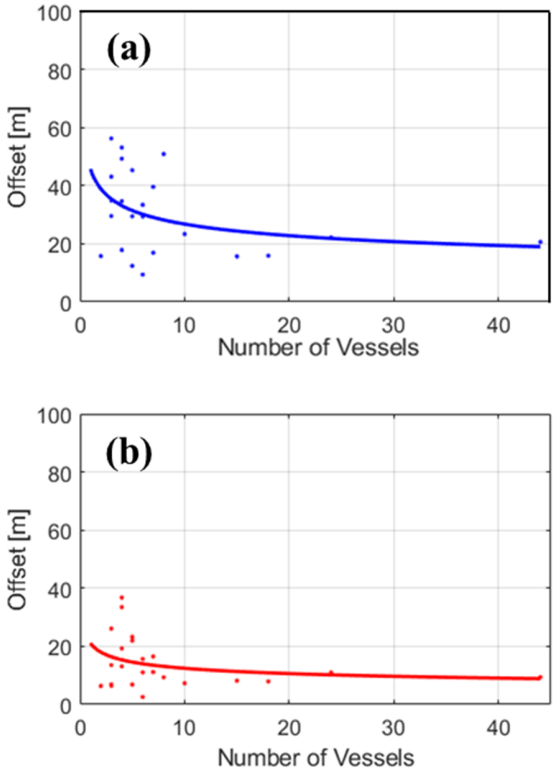

Fig. 4. Relation between the number of AIS-assisted vessels in HiSEA-1 image coverage and residual offset after the proposed geo-location enhancement algorithm (a) without and (b) with static AIS information.

AIS information, geometric calibration offset was significantly enhanced even without utilizing GCPs.

In addition, enhancement on conventional SAR satellites, COSMO-SkyMed and Sentinel-1, was equally conducted. Synergistically using terrain information and atmospheric phase correction yielded residual offset of 2.5 m for Sentinel-1 IW mode [14] and 10 m for COSMO-SkyMed Himage mode [15]. As described in Fig. 3, facilitating static AIS information, both satellite SAR satisfied the residual offset presented in [14] and [15]. Such mitigation of geo-location in ocean outperformed the accuracy of conventional ellipsoid correction based on Range-Doppler model in ocean using TerraSAR-X, demonstrating approximately 300 m of geo-location offset [6]. Fig. 4 describes the relationship between the number of vessels with AIS information in SAR image coverage and the residual offset of HiSEA-1 images. For images with the large number of vessels in its region tended to have smaller residual offset. Such inaccuracy was allegedly caused by vessel height of larger containers, where height of the vessel superstructure from sea level causes the focus of target vessels to be shifted to near range.

Utilizing preprocessed AIS information and estimating the shift from the nearest detected vessel, positioning offset from ellipsoid correction in SAR images was effectively mitigated so that it can be implemented to practical maritime surveillance without the aid from GCPs. Accompanied by the residual correction which varies within spatial coverage, the proposed algorithm can be applied not only to a precise geometric calibration, but also to the real-time vessel monitoring from remote sensing apparatus.

V. Conclusion

An algorithm which investigated the enhancement of geometric positioning offset, where GCPs were inaccessible, was proposed and implemented to SAR images acquired in maritime regions. Repetitive comparison between AIS information and detected vessels was conducted, while shifting the corresponding SAR image with respect to it. The estimated positioning offset was clearly reduced after utilizing the algorithm, especially when using information from AIS sensor arrangement. Consecutive studies are able to focus on mitigation of the residual error terms before being implemented to real-time maritime surveillance.

Acknowledgment

The authors would like to thank the Ministry of Oceans and Fisheries, South Korea, for providing automatic identification system (AIS) data.

References

[1] I. Petillot et al., "Radar-coding and geocoding lookup tables for the fusion of GIS and SAR data in mountain areas," *IEEE Geosci. Remote Sens. Lett.*, vol. 7, no. 2, pp. 309–313, Apr. 2010.
[2] S. Wang, G. Yang, and L. Wang, "An improve hybrid calibration scheme for strapdown inertial navigation system," *IEEE Access*, vol. 7, pp. 151669–151681, 2019.
[3] H. Qi and J. B. Moore, "Direct Kalman filtering approach for GPS/INS integration," *IEEE Trans. Aerosp. Electron. Syst.*, vol. 38, no. 2, pp. 687–693, Apr. 2002.
[4] M. Shimada, "Ortho-rectification and slope correction of SAR data using DEM and its accuracy evaluation," *IEEE J. Sel. Topics Appl. Earth Observ. Remote Sens.*, vol. 3, no. 4, pp. 657–671, Dec. 2010.
[5] S. Montazeri, F. Rodríguez González, and X. Zhu, "Geocoding error correction for InSAR point clouds," *Remote Sens.*, vol. 10, no. 10, p. 1523, Sep. 2018.
[6] W. Linglin, L. Yongxin, and Z. Hui, "A fast SAR image position algorithm for maritime target location," in *Proc. Chin. Control Decis. Conf. (CCDC)*, May 2016, pp. 3534–3538, doi: 10.1109/CCDC.2016.7531595.
[7] J.-I. Hwang, S.-H. Chae, D. Kim, and H.-S. Jung, "Application of artificial neural networks to ship detection from X-band Kompsat-5 imagery," *Appl. Sci.*, vol. 7, no. 9, p. 961, Sep. 2017.
[8] J. Song, D.-J. Kim, S. An, and J. Kim, "Restoration of authentic position of unidentified vessels in SAR imagery: A deep learning based approach," *IEEE J. Sel. Topics Appl. Earth Observ. Remote Sens.*, vol. 15, pp. 1064–1078, Jan. 2022.
[9] X. Wang, G. Li, X.-P. Zhang, and Y. He, "A fast CFAR algorithm based on density-censoring operation for ship detection in SAR images," *IEEE Signal Process. Lett.*, vol. 28, pp. 1085–1089, 2021.
[10] G. Tang, S. Liu, I. Fujino, C. Claramunt, Y. Wang, and S. Men, "H-YOLO: A single-shot ship detection approach based on region of interest preselected network," *Remote Sens.*, vol. 12, no. 24, p. 4192, Dec. 2020.
[11] M.-K. Lee, Y.-S. Park, S. Park, E. Lee, M. Park, and N.-E. Kim, "Application of collision warning algorithm alarm in fishing Vessel's waterway," *Appl. Sci.*, vol. 11, no. 10, p. 4479, May 2021.
[12] Q. Hu, L. Xu, and X. Cheng, "A CORS-based differential correction approach for AIS mobile stations," *Sensors*, vol. 18, no. 11, p. 3626, Oct. 2018.
[13] G. Schreier, D. Kosmann, and A. Roth, "Design aspects and implementation of a system for geocoding satellite SAR-images," *ISPRS J. Photogramm. Remote Sens.*, vol. 45, no. 1, pp. 1–16, May 1990.
[14] K. Schmidt, J. Reimann, M. Schwerdt, and N. T. Ramon, "Geometric accuracy of Sentinel-1A and 1B derived from SAR raw data with GPS surveyed corner reflector positions," *Remote Sens.*, vol. 10, no. 4, p. 523, Mar. 2018.
[15] A. Schubert, D. Small, M. Jehle, and E. Meier, "COSMO-Skymed, TerraSAR-X, and RADARSAT-2 geolocation accuracy after compensation for Earth-system effects," in *Proc. IEEE Int. Geosci. Remote Sens. Symp.*, Jul. 2012, pp. 3301–3304.
[16] A. Bochkovskiy, C.-Y. Wang, and H.-Y. M. Liao, "YOLOv4: Optimal speed and accuracy of object detection," 2020, *arXiv:2004.10934*.